Published online 20 October 2022 *Nucleic Acids Research, 2022, Vol. 50, No. 19* ***11387–11400***
https://doi.org/10.1093/nar/gkac870

G-quadruplex-guided RNA engineering to modulate CRISPR-based genomic regulation

Xingyu Liu†, Shuangyu Cui†, Qianqian Qi†, Huajun Lei†, Yutong Zhang, Wei Shen, Fang Fu, Tian Tian* and Xiang Zhou

Key Laboratory of Biomedical Polymers of Ministry of Education, College of Chemistry and Molecular Sciences, Hubei Province Key Laboratory of Allergy and Immunology, Wuhan University, Wuhan 430072, Hubei, China

Received June 28, 2022; Revised September 23, 2022; Editorial Decision September 23, 2022; Accepted September 27, 2022

ABSTRACT

It is important to develop small moelcule-based methods to modulate gene editing and expression in human cells. The roles of the G-quadruplex (G4) in biological systems have been widely studied. Here, G4-guided RNA engineering is performed to generate guide RNA with G4-forming units (G4-gRNA). We further demonstrate that chemical targeting of G4-gRNAs holds promise as a general approach for modulating gene editing and expression in human cells. The rich structural diversity of RNAs offers a reservoir of targets for small molecules to bind, thus creating the potential to modulate RNA biology.

INTRODUCTION

CRISPR stands for clustered regularly interspaced short palindromic repeats (1). With appropriately designed guide RNA (gRNA), CRISPR-associated protein (Cas) can cut the target sequence at specific positions *in vitro* and *in vivo* (2–4). Current investigations established the CRISPR/Cas9 system as a cutting-edge tool enabling precise genomic editing (3,5). Gene expression can also be activated or suppressed using CRISPR systems (6–8). A concern of this technology is that the CRISPR complexes, once introduced into cells, are difficult to restrain (9). On-demand activation of CRISPR/Cas9 was developed to control this system (10–15). However, once the pro-caged system is activated, the prolonged activity can lead to toxicity and other adverse effects. There are currently limited means to suppress CRISPR/Cas9 in cells (16–18), leading to practical difficulties and safety concerns. Moreover, the repertoire of small-molecule CRISPR inhibitors is insufficient for many applications.

The gRNA is an important component of the CRISPR/Cas9 system and can be provided with different formats (2,3). For natural CRISPR/Cas9, CRISPR RNA (crRNA) functions with *trans*-activating crRNA (tracrRNA) and directs Cas9 protein to the target positions (2). The core components of these RNAs can be combined into a single hybrid gRNA (sgRNA) to simplify the use of CRISPR/Cas9. The crystal structure studies of Cas9–gRNA complexes revealed that several structural components are formed in both sgRNA and tracrRNA (19,20). These structural components, including a repeat:anti-repeat duplex, stem–loops 1–3 and the linkers, are essential for the formation of the functional complexes (19). We realised that structural recognition can be exploited for specific RNA modulation (21). Some important studies demonstrated the conformational transition between different structures within an RNA molecule (22,23). Inspired by these facts, we considered developing a gRNA-targeting strategy by introducing switching units into gRNAs. It is known that guanine (G)-rich nucleic acids are capable of forming a stable G-quadruplex (G4) structure via Hoogsteen hydrogen bonds (24–26). To date, a number of small molecules have been identified as excellent G4-stabilizing ligands (27–30). We hypothesized that chemical targeting of RNA G4 units can be used to regulate the activity of a properly engineered RNA of interest.

Here we describe our design and development of G4-guided RNA engineering to introduce an RNA G4 unit and its small-molecule ligands that can be applied to establish drug sensitivity into both *in vitro* and intracellular applications. Using bioinformatics analysis, we first identify a structural component with a high G content in the 3′ end of the scaffold sequence for both sgRNA and tracrRNA (G4-sgRNA in Figure 1A, G4-tracrRNA in Supplementary Figure S1). We provide direct evidence for the competitive formation of a stem–loop and G4 structure within model RNAs. Parallel sequence modifications are performed to generate gRNA variants with potential G4-forming units. We demonstrate that these intended modifications are well tolerated for CRISPR/Cas9. We further demonstrate that these sequence changes can make gRNAs responsive to

*To whom correspondence should be addressed. Email: ttian@whu.edu.cn
†The authors wish it to be known that, in their opinion, the first four authors should be regarded as Joint First Authors.

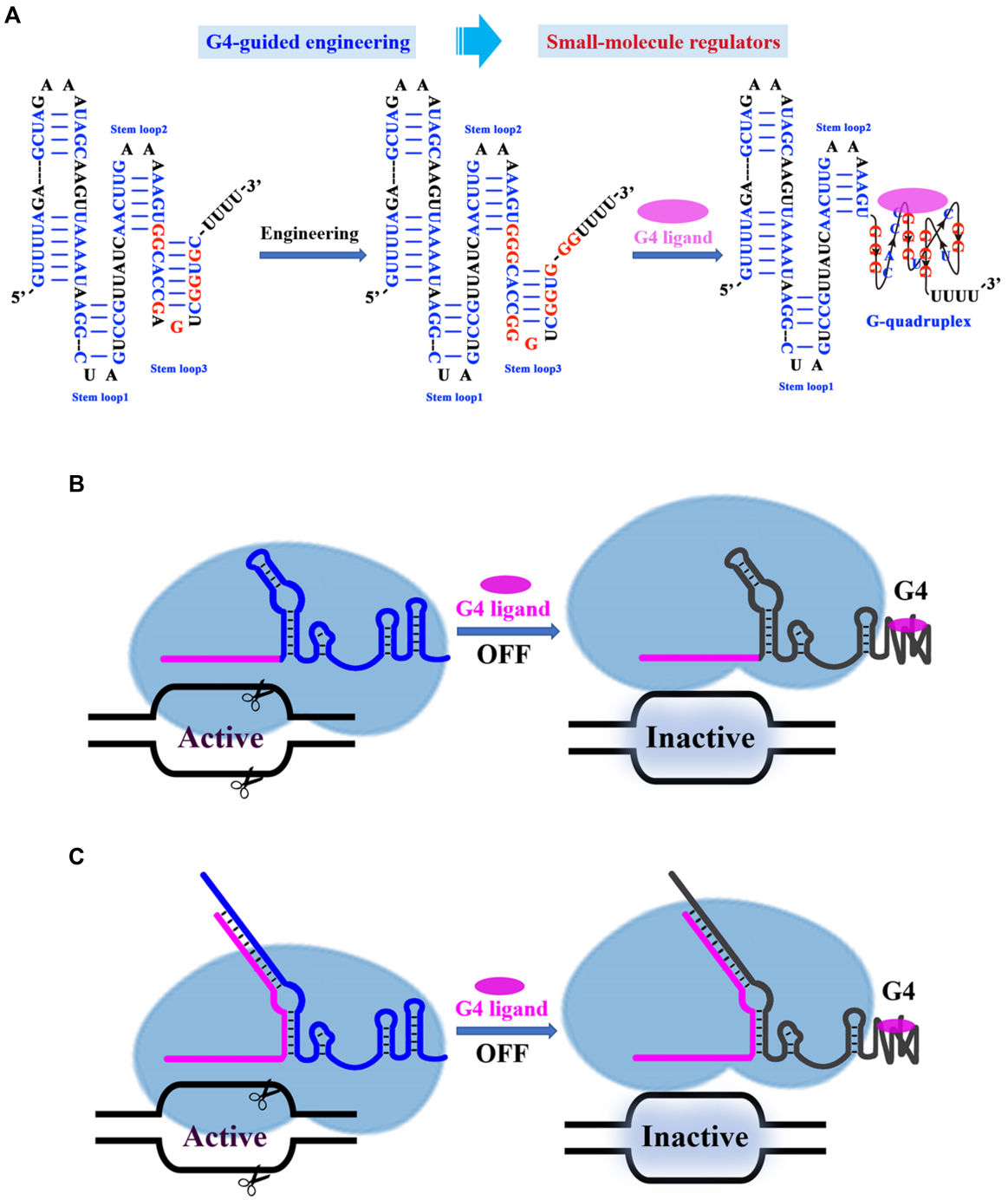

Figure 1. Schematic illustration of the design and workflow. (**A**) G4-guided engineering of sgRNAs. The sgRNA scaffold contains multiple well-defined structural motifs, including a repeat:anti-repeat duplex and three stem–loops. Stem–loop 3 was chosen as an optimal motif for engineering sgRNAs. (**B,C**) CRISPR/Cas9 functions are controlled by harnessing interactions between small molecules and G4-sgRNAs (B) or G4-tracrRNAs (C).

small-molecule ligands both *in vitro* and in cells (Figure 1B, C). Finally, we conclude that with this approach of rational gRNA modifications along with the use of G4 ligands, the level of gene editing and expression can be modulated in human cells. Our strategy holds promise in light of designs more widely applied to modulate other functional RNA systems in biology.

MATERIALS AND METHODS

Circular dichroism (CD) studies

Each RNA was annealed 24 h before the CD study by heating the sample to 90 °C for 5 min in a buffer (10 mM Tris–HCl pH 7.0 and various concentrations of KCl) then slowly cooled to room temperature over 3 h and stored at 4 °C

overnight. After adding each G4 ligand, samples were thoroughly mixed and equilibrated for 1 h before CD measurements. CD spectra were collected on a JASCO J-810 CD spectrophotometer using a quartz cuvette with a 1.0 mm path length. Each trace was the result of the average of four scans taken with a step size of 0.5 nm, a time-per-point of 1.5 s and a bandwidth of 2 nm. Using the JASCO Spectra Analysis software, spectra were converted to mean residue molar ellipticity and smoothed by the means-movement method using a convolution width of five. A blank sample, consisting only of buffer, was treated in an identical manner and subtracted from the collected data.

UV melting studies

UV melting assay was performed using a Jasco-810 spectropolarimeter equipped with a water bath temperature-control accessory. The measurements are performed using a 1.0 mm path length cell and samples containing each model RNA (15 μM) in 10 mM Tris–HCl (pH 7.0) and various concentrations of KCl. UV melting profiles were recorded by using a heating rate of 0.2°C/min and the absorbance values were collected every 1°C. The melting point (T_m) corresponds to the mid-transition temperature, which was determined by the maximum of the first derivative of the absorbance as a function of temperature. CD melting was performed using the following parameters: wavelength, 264 nm; bandwidth, 4 nm; temperature range, 4–95 °C; temperature step, 1 °C; dead band, 0.33 °C; equilibrating time, 0.5 min; averaging time, 20–30 s.

Native polyacrylamide gel electrophoresis (PAGE) analysis

PAGE analysis was performed in a vertical electrophoretic apparatus (DYCZ-22A; Liuyi Instrument Factory, Beijing, China) with a temperature control module (4.0°C). The resolving gel has a high concentration (20%) of acrylamide (19 : 1 monomer to bis ratio). The fluorescein-labeled RNA sample was prepared in a buffer (10 mM Tris-HCl, pH 7.0) containing 70 mM KCl. About 10 ng of RNA were loaded for analysis (300 V, 4 h). Polyacrylamide gels were imaged on a Pharos FX Molecular imager (Bio-Rad, USA) in fluorescence mode.

Nuclear magnetic resonance (NMR) study

^{1}H-NMR spectra were recorded at 298 K using a 600 MHz Bruker Avance DRX-600 spectrometer equipped with a cryogenic TCI ATM probe. The RNA samples were dissolved in 10 mM phosphate-buffered saline (PBS; pH 7.0) containing 100 mM KCl and 10% D_2O at a final concentration of 0.5 mM. The samples were annealed after heating at 90°C for 4.0 min and slowly cooled to 25°C. NMR spectra in water were recorded using excitation sculpting for water suppression with an acquisition time of 1.5 s, and a relaxation delay of 2.5 s at 25°C.

Generation of G4-sgRNAs and G4-tracrRNAs

In vitro transcription reactions were performed to make each sgRNA and tracrRNA. An overlap extension is performed to assemble smaller DNA fragments into a larger sequence, which was used for making each sgRNA and tracrRNA (11). The templates for transcription were ordered as complementary oligomers and contained a T7 promoter at the 5′ end of the gRNA sequence. For sgRNA preparation, the forward primer was designed to contain T7 promoter (5′-TAATACGACTCACTATA-3′), variable guide sequence and the first 31 nt of the conserved region of the sgRNA scaffold (sg-SLX4IP-F, sg-HPRT1-F or sg-HBEGF-F). The reverse primer was designed to contain the reverse complement of the conserved region of the sgRNA scaffold (sgRNA-R, sgRNA-G4a-R, sgRNA-G4b-R or sgRNA-G4c-R in Supplementary Table S1). The oligomers were mixed at an equal concentration at 500 ng/μl, heated to 95 °C for 5 min and slow cooled to room temperature. Transcription reactions were performed using 300 ng polymerase chain reaction (PCR) fragments following the protocol provided in the Transcript Aid T7 High Yield Transcription kit (product# K0441, Thermo Fisher Scientific). Afterward, the DNA template was degraded by the addition of 1 U of DNase I for every 20 μl of reaction and incubated at 37°C for 15 min. The reaction was cleaned up using the RNA Clean and Concentrator-25 kit (Zymo Research Corporation, CA, USA) according to the manufacturer's instructions, eluted in 100 μl of RNase-free water and precipitated with 10 μl of 3 M sodium acetate and 250 μl of 100% ethanol overnight at –20°C. The sample was centrifuged at 4 °C for 30 min; the pellet was washed with 70% ethanol, resuspended in 20 μl of nuclease-free water and stored at –80 °C until ready to use. Purified RNA was quantified by measuring absorbance at 260 nm, and extinction coefficients were calculated using nearest neighbor approximations and Beer's Law.

For tracrRNA preparation, the forward primer was designed to contain the T7 promoter and the first 46 nt of the tracrRNA scaffold (tracrRNA-F); the reverse primer was designed to contain the reverse complement of the tracrRNA scaffold (tracrRNA-R, tracrRNA-G4a-R, tracrRNA-G4b-R or tracrRNA-G4c-R in Supplementary Table S1). For overlap extension and *in vitro* transcription reaction, the conditions were the same as the above sgRNA protocol. The crRNAs were ordered as HPLC-purified RNA oligomers, resuspended in nuclease-free water at 100 μM concentration and stored at –80 °C until needed.

Chemical targeting of *in vitro* transcribed (IVT) G4-sgRNAs for controlling gene editing

PX165 (pSpCas9) was obtained from Addgene (plasmid# 48137) (31). A dimethylsulfoxide (DMSO) solution of each G4 ligand was resuspended in 10% fetal bovine serum (FBS)-containing growth medium and thoroughly mixed before adding to the cells. HeLa cells were cultured in complete media, Gibco™ Dulbecco's modified Eagle's medium (DMEM), High Glucose medium (Thermo Fisher Scientific), 10% (v/v) Gibco™ FBS (Thermo Fisher Scientific) and 1% penicillin/streptomycin (Invitrogen), at 37°C in a 5% CO_2 incubator (32). One day prior to transfection, 4 × 10^5 HeLa cells per well were seeded into a 6-well plate containing 0.5 ml of medium. HeLa cells were transfected with 2.5 μg of PX165 plasmid using a standard transfec-

tion protocol. In brief, PX165 plasmid was mixed in 125 μl of DMEM. Thereafter, an equal volume of DMEM with Lipofectamine 3000 transfection agent (5.0 μl) was added and incubated for 15 min. The complex was subsequently added dropwise to the cells. After 4 h of incubation, cells were treated with Lipofectamine 3000 loaded with endogenous gene-targeting sgRNAs (2.5 μg/well). After an incubation time of 4 h, the medium was changed to complete medium supplemented with appropriate concentrations of each G4 ligand or DMSO. For analysis of gene editing efficiency, genomic DNA was isolated from experimental and control samples at 24 h post-treatment using the Qiagen DNeasy Blood and Tissue Kit.

Isolated genomic DNA was subjected to PCR amplification using target site-specific primer sets employing PrimeSTAR HS DNA Polymerase. The PCR program was set as follows: initial denaturation at 94°C for 15 s; and 35 cycles consisting of 10 s of denaturation at 98°C, 1 min of annealing and extension at 68°C. Final extension was set at 72°C for 5 min. The amplicons were purified using the Zymo Research DNA Clean and Concentrator Kit. The target editing efficiency and inhibition thereof were quantified by T7E1 assay. The reaction was quenched by adding SDS-containing loading dye and loaded onto a 1.5% agarose gel containing 1.5× Super GelRed for visualization (100 V, 1.5 h). The band intensity for the cleavage product band was divided by the combined intensity of the cleavage product and uncut substrate bands, and is reported as fraction cleaved. For negative controls, either the PX165 plasmid or the sgRNA was omitted.

Ribonucleoprotein (RNP) study

EnGen Spy Cas9 NLS protein (30 pmol) with 45 pmol sgRNAs was electroporated into 8×10^5 HeLa cells before the treatment with pyridostatin (PDS). The electroporation was performed using a Lonza 4D-Nucleofector X unit in 100 μl of SE buffer employing SE-CN114 as the program according to the manufacturer's protocol. Immediately after transfection, cells were treated with appropriate concentrations of G4 ligand and incubated for an additional 24 h at 37°C with 5% CO_2. The target editing efficiency and inhibition thereof were quantified by T7E1 assay.

G4-guided engineering of an RNA-expressing cassettes in all-in-one plasmid

pSpCas9(BB)-2A-Puro (PX459) V2.0 was a gift from Feng Zhang (Addgene plasmid # 62988). A starting PX459 plasmid was used to construct each G4-containing plasmid (PX459-G4x, x indicates a, b or c). Sequence modifications were generated through overlap extension PCR of the region between unique restriction sites (PciI/SnaBI) of PX459, and two primer pairs [forward primer in upstream region (G4-up-F), reverse primer in upstream region (G4x-up-R); forward primer in downstream region (G4x-down-F), reverse primer in downstream region (G4-down-R)] were used. The two purified fragments were used in the overlap extension PCR to produce the fused fragment containing G4-encoding sequences. Assembled PCR products were amplified with Pyrobest™ DNA Polymerase using forward and reverse oligonucleotides (G4-up-F and G4-down-R) with homology upstream or downstream of the PciI and SnaBI restriction sites, respectively. PX459 plasmid was digested with PciI/SnaBI to remove the original sgRNA cassette. The linearized plasmids and the assembled PCR products of the correct lengths were assembled with the in-fusion cloning method to produce the target plasmid PX459-G4x. Constructed plasmids were sequenced to confirm the replaced strand region using the primer 5′-CTTTTGCTGGCCTTTTGCTCA-3′.

Chemical targeting of plasmid-encoded G4-sgRNAs for controlling gene editing

To introduce target sites into the cloning site of each construct, we use a cloning strategy that ligates two annealed oligos into the backbone that has been digested with BbsI (PX459, PX459-G4a, PX459-G4b or PX459-G4c). Forward and reverse oligonucleotides containing the guide sequences for *SLX4IP* and *HPRT1* with appropriate overhangs were annealed by mixing 100 pmol of each pair and then incubated at 90°C for 5 min and slowly ramped to room temperature. The sequence of the insert was confirmed by Sanger sequencing.

We plated 4×10^5 HeLa cells in each well of a 6-well plate. Cells were transfected with 2.5 μg of each complete plasmid using 5 μl of Lipofectamine 3000. After 4 h of transfection, the medium of the 'control groups' and the 'experimental groups' was replaced by the same medium, but in the 'experimental groups' it contained appropriate concentrations of PDS. Then, the groups of cells were cultured for another 24 h. The cells were then lysed and genomic DNA was extracted and PCR-amplified around the target locus. Finally, the genomic modification efficiency was determined by using the T7E1 assay.

Chemical targeting of G4-sgRNAs for controlling gene expression

A starting scFv-GCN4-GFP-VP64 plasmid (a gift from Ron Vale, Addgene plasmid # 60904) was used to construct the one with the KRAB repressor (scFv-GCN4-GFP-KRAB). Fused fragments were generated through overlap extension PCR of the region between unique restriction sites (BamHI/SpeI) of scFv-GCN4-GFP-VP64, and two primer pairs [forward primer in upstream region (scFv-KRAB-UP-F), reverse primer in upstream region (scFv-KRAB-UP-R); forward primer in downstream region (scFv-KRAB-down-F), reverse primer in downstream region (scFv-KRAB-down-R)] were used. The two purified fragments were used in the overlap extension PCR to produce the fused fragment. Assembled PCR products were amplified with Pyrobest™ DNA Polymerase using forward and reverse oligonucleotides (scFv-KRAB-UP-F and scFv-KRAB-down-R) with homology upstream or downstream of the BamHI and SpeI restriction sites, respectively. The assembled PCR products and the digested scFv-GCN4-GFP-VP64 plasmids (BamHI/SpeI) were assembled with the in-fusion cloning method to produce the target plasmid scFv-GCN4-GFP-KRAB.

To determine the levels of *CXCR4* transcriptional control, HeLa cells were seeded at 4×10^5 cells/well in a 6-well plate and transfected with dCas9-SunTag (a gift from Ron Vale, Addgene plasmid # 60903) together with either scFv-GCN4-GFP-VP64 or scFv-GCN4-GFP-KRAB for 4 h. The dose of each plasmid was 2.5 μg/well. Cells were then treated with Lipofectamine 3000 loaded with sgRNA targeting the *CXCR4* promoter (sg-CXCR4 in Supplementary Table S1) for 4 h. The sgRNA dose was 2.5 μg/well of each sgRNA. HeLa cells were then treated with various concentrations of PDS. At 24 h post-treatment, total RNA was isolated with Trizol (Ambion), and cDNA was synthesized using the cDNA Superscript First Strand Synthesis Kit (TaKaRa). The target transcriptional activation and inhibition thereof were quantified by quantitative PCR (qPCR primers in Supplementary Table S1). Three biological replicates were performed for each condition.

RESULTS

The design of G4-guided RNA engineering

The goal of this study was to develop small molecule-based methods to control CRISPR-mediated gene editing and expression. It is known that nucleic acids can be programmed to adopt pre-defined structures by modifying their primary sequence (33). The reliance of Cas9 on gRNAs suggests that they may serve as a viable platform for our purpose (19). In this study, we use the conventional definitions to avoid confusion: gRNA is the term that describes both gRNA formats, including sgRNA and crRNA:tracrRNA. Both sgRNA and tracrRNA contain a conserved scaffold sequence needed for binding of Cas9. This scaffold sequence therefore represents an ideal model to examine our concepts. Recent studies have studied the formation of RNA G4 in competition with helix-based structures in long stretches of RNA (22,23). In this respect, we considered to explore and exploit the use of a G4-triggered structural switch for manipulating gRNA functions.

The sequence engineering should be performed in such a way that the original function of gRNA is not perturbed. G-tracts are essential to the formation of the G-tetrads that are fundamental aspects of G4 structure (34). Most relevant to this step are the following two considerations: a relatively high G content; and a high frequency of continuous G runs (24). We therefore conducted G content analysis of gRNA scaffold to identify regions which tend to be richer in G (Supplementary Figure S2). The regional G content was calculated by dividing the whole gRNA scaffold (80 nt) into 15 nt windows with 1 nt steps (left part in Figure 2A and Supplementary Figure S3A). Figure 2B and Supplementary Figure S3B show the distributions of G contents of each region along the scaffold. The results demonstrate that the heterogeneity in G content appears to be evident. There is a greater G richness in stem–loop 3 at the 3′ tail compared with the others. Engineering of this region holds the promise of reducing much disturbance. We therefore set out to engineer this motif through introduction of G4-forming units. Two types of modifications are adopted: (i) the substitutions of G for non-G sites and (ii) the insertion of extra G at specific positions (right part in Figure 2A and Supplementary Figure S3A). In the absence of G4 ligand, the active stem–loop predominates and maintains high gRNA activity. However, in the presence of G4 ligands, G4 will be stabilized by ligand binding energy and disrupts the original stem–loop, resulting in loss of gRNA function.

G4-guided engineering of model stem–loop 3

The above G content analysis demonstrates that the sequence of stem–loop 3 represents a structurally distinct target (R-SL3 in Figure 3A). Considering the highly polymorphic nature of the gRNA sequence, this short sequence is examined first. CD spectroscopy is used to quickly study the global structural features of an RNA under different conditions (35). If there are differences between the spectra of the RNA recorded in two different conditions (plus G4 ligand and minus G4 ligand), then it would be indicative of some binding-induced structural change such as stem–loop to G4 transitions (36). To this aim, each RNA in the absence and presence of G4 ligands is examined for comparison (Figure 3B, C; Supplementary Figures S4 and S5). There are only slight peak height differences at 260 nm when wild-type R-SL3 was treated with G4 ligands (Supplementary Figure S4A). This phenomenon may suggest subtle structural differences of R-SL3 between these two conditions.

In this study, G4-guided engineering of stem–loop 3 is performed to generate different variants (R-SL3-G4a, R-SL3-G4b and R-SL3-G4c in Figure 3A). In the R-SL3-G4a variant, two substitution sites were chosen to introduce a G4 motif (C76G/A68G), while R-SL3-G4b and R-SL3-G4c have extra G sites in the G-rich stretches of the predicted G4-forming sequence of stem–loop 3 (60 + G/75 + G). We proceeded to characterize the possible structural transition of engineered RNAs (37). For the CD study, each RNA was incubated in the presence of different concentrations of KCl, with and without G4-interactive agent. The treatment of R-SL3-G4a with G4 ligands caused changes in its CD spectrum indicative of a global conformational transition (Supplementary Figures S4C and S5A). For R-SL3-G4b and R-SL3-G4c with additional G residues at the terminal positions, the G4 ligand-induced increase of absorbance intensity at 260 nm became more pronounced (Figure 3C; Supplementary Figure S4, S5). Moreover, the treatment with each G4 ligand markedly increased the T_m of R-SL3-G4c with additional G sites, indicating evident RNA G4 stabilization at physiological ionic strength (Figure 3D; Supplementary Figure S4H). For this engineered sequence, the stem–loop and G4 might co-exist in the absence of G4 ligands, whereas G4 is predictably preferred to the stem–loop in the presence of G4 ligands.

Native PAGE was performed to seek more evidence for the structural switch induced by G4 ligand (38,39). In this study, each model RNA was fluorescently labeled to facilitate analysis (R-SL3-FAM, R-SL3-G4a-FAM, R-SL3-G4b-FAM and R-SL3-G4c-FAM in Supplementary Table S1). As demonstrated in Figure 3E, the engineered RNA migrated at a similar rate compared with the wild-type control in the absence of G4 ligands. This phenomenon demonstrated that the engineering does not significantly affect the original RNA fold. Further results demonstrate that the mi-

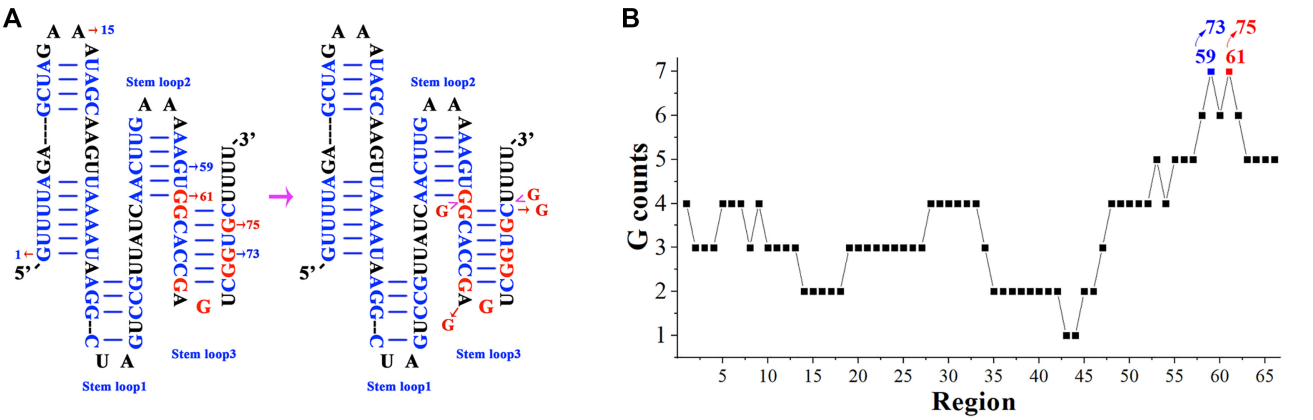

Figure 2. Sequence and structure analysis of gRNA scaffold (sgRNA). (**A**) Using structure-based design principles, the 3′ end of sgRNA is engineered by rationally designed nucleotide substitutions and insertions. The engineering sites are indicated in red. (**B**) The G content for each region was calculated as a simple count. The histogram shows a significantly higher G content in the sgRNA scaffold when looking at the 3′ region compared with that of the rest of the regions.

gration rate of engineered RNAs is significantly retarded upon the addition of G4 ligands (Figure 3E; Supplementary Figure S6). We propose that the differential migration can be explained by the charge or the conformational changes of the engineered RNA after the formation of stable complexes with the G4 ligands. In addition, almost no retardation was detectable after incubation of the wild-type RNA with G4 ligands. These results are consistent with the CD data, where the engineered RNAs demonstrate higher binding affinity toward G4 ligands than the wild-type sequence. The binding-induced structural change of the engineered sequence was further supported by 1D-NMR experiments (40–42). The ^{1}H-NMR spectrum of R-SL3-G4c in the presence of pyridostatin derivative (PDP) demonstrated broad imino peaks within the 10.0–11.5 ppm region (Figure 3F), which are characteristic of the Hoogsteen hydrogen bonds of G-quartets.

Chemical targeting of G4-gRNA for modulating CRISPR/Cas9

The above studies demonstrate that G4 ligands can specifically induce a stem–loop to G4 transition related to stem–loop 3. We are encouraged to test the efficiency of using G4 ligands in combination with G4-gRNAs to modulate CRISPR/Cas9. We designed the guide sequences of sgRNAs to target the selected positions within different target DNAs (hypoxanthine phosphoribosyltransferase 1, *HPRT1* gene in Supplementary Figure S7A; the SLX4-interacting protein, *SLX4IP* gene in Supplementary Figure S7B; and heparin-binding EGF-like growth factor, *HBEGF* gene in Supplementary Figure S7C) (11,32,43,44). Taking the *SLX4IP*-targeting sgRNAs as examples, we designed and generated a series of G4-sgRNAs (sg-SLX4IP-G4a, sg-SLX4IP-G4b and sg-SLX4IP-G4c in Supplementary Table S1). From the structural point of view, sg-SLX4IP-G4a represents a variant with double nucleotide substitutions, and the other two variants (sg-SLX4IP-G4b and sg-SLX4IP-G4c) carry both substitutions and insertions in their sequences. Sanger sequencing of individual variants was performed to confirm the correct engineering of sgRNAs (Figure 4A; Supplementary Figures S8 and S9A).

Engineered CRISPR/Cas9 comprises an sgRNA and Cas9 nuclease, which together form an RNP complex (19,45). Good functional activity of a G4-sgRNA requires proper interactions between it and Cas9. The interaction between G4-sgRNA and Cas9 protein can be evaluated through an electrophoretic mobility shift assay (EMSA) (46). We used a Halo-Tagged dCas9 (nuclease-dead Cas9), in which the Halo tag can be labeled by Halo ligands conjugated to a fluorescent dye (47). Our results show that G4-sgRNAs exhibit appreciable binding to dCas9 relative to the control sgRNAs (Figure 4B; Supplementary Figure S10). After treatment with increasing concentrations of G4 ligand, the band corresponding to the binary complexes (sgRNA–dCas9) gradually diminished. These results demonstrate that the formation of Cas9–gRNA complexes can be influenced by binding-induced changes in RNA topology.

We proceeded to investigate whether these gRNA variants can be used to support Cas9-mediated DNA cleavage. The most commonly used Cas9 nuclease is the one originating from *Streptococcus pyogenes* (2,48). As the starting point, it is important to determine the range of tolerance of Cas9 to sequence modification of gRNAs. For our purpose, each target DNA was amplified by PCR from human genomic DNA. When the Cas9 was complexed with each G4-sgRNA, the target DNA was cut with an efficiency comparable with that observed for the wild-type sgRNA (Figure 4C: Supplementary Figure S11A, B). In parallel to the sgRNA variants, we also generated three tracrRNA variants, which differ from each other by nucleotide substitutions and insertions (tracrRNA-G4a, tracrRNA-G4b and tracrRNA-G4c in Supplementary Figure S9B). When combined with each crRNA and Cas9, we found no significant difference in relative overall activity of these sequence-modified tracrRNAs, compared with the standard wild-type sequence (Figure 4D; Supplementary Figure S11C, D). These results together demonstrate that gRNAs are quite tolerant of our intended sequence modifications in stem–loop 3.

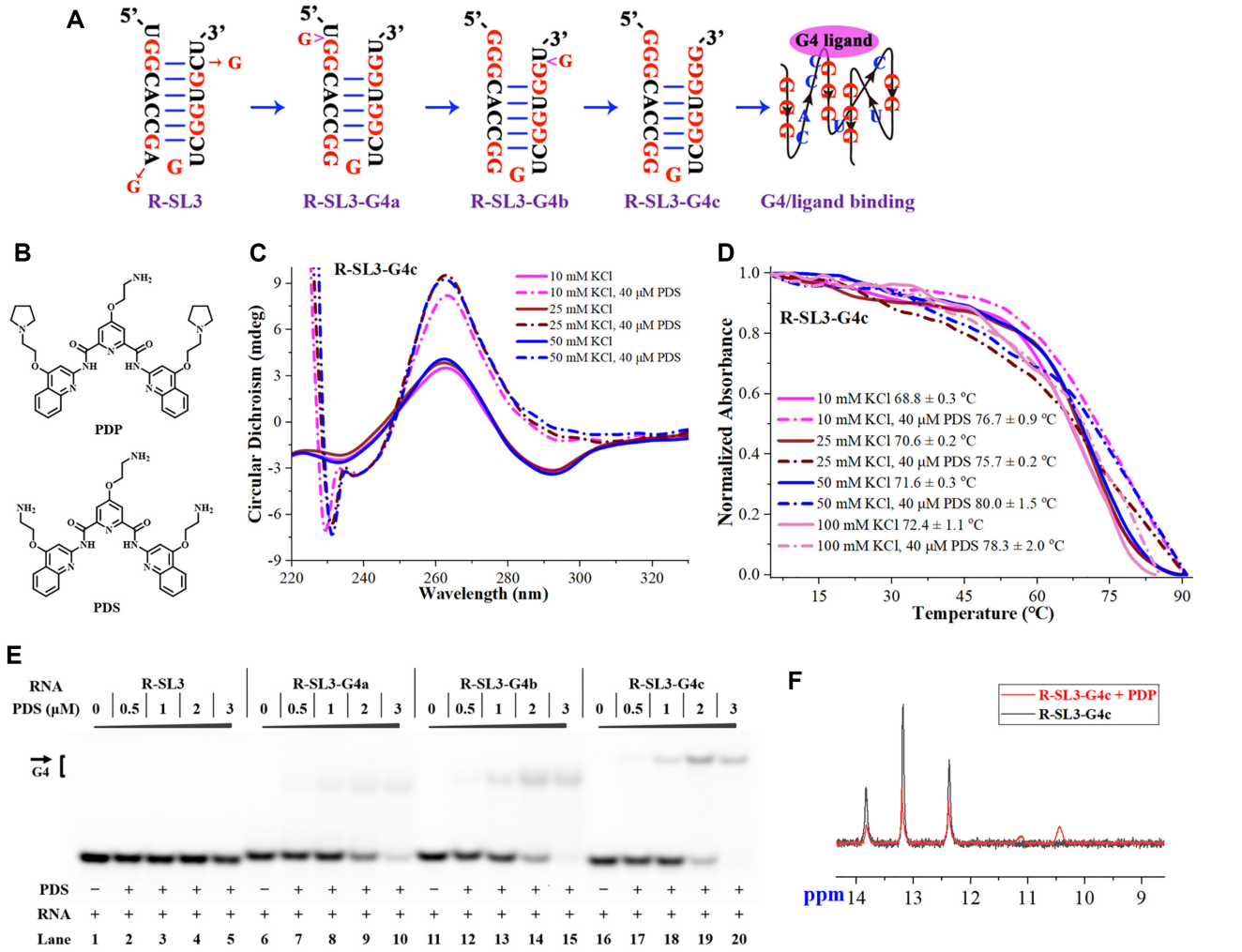

Figure 3. G4-guided engineering of model RNAs (stem–loop 3). Experiments were performed as described in the Materials and methods. All samples were tested in three biological replicates. An image of representative data is shown here. (**A**) G4-guided engineering of model RNAs. (**B**) The structure of representative G4 ligands. (**C**) Recording the spectrum of R-SL3-G4c in the presence of PDS and then comparing with the spectrum obtained in the absence of PDS. All experiments were performed in a Tris–HCl buffer (10 mM, pH 7.0) containing KCl. Total RNA strand concentration was 15 μM. (D) CD melting curves for R-SL3-G4c in the absence or presence of PDS. All normalized melting curves were temperature overlaid for illustration purposes. (E) Native PAGE analysis of RNA strands before and after treatment with PDS. Lanes 1, 6, 11, 16, the untreated RNAs; lanes 2–5, 7–10, 12–15, 17–20, the PDS-treated RNAs. (**F**) 1H-NMR demonstration of G4 structures of R-SL3-G4c in the presence of pyridostatin derivative (PDP).

We next investigate the propensity of G4 ligands to modulate the function of G4-gRNAs. In this study, CRISPR/Cas9 complexes were exposed to different concentrations of each G4 ligand. We demonstrate that the Cas9-mediated DNA cleavage was significantly inhibited by treating sg-HPRT1-G4a with each G4 ligand (Supplementary Figure S12A). We also demonstrated that PDS is more capable of disrupting the function of G4-sgRNAs when compared with PDP. The reason for this discrepancy in anti-CRISPR activity between PDS and PDP against G4-sgRNAs is not clear.

Given the successful inhibition of sg-HPRT1-G4a by each G4 ligand, we moved to test whether rational optimization of G4 elements can enhance the sensitivity of G4-sgRNAs to chemical stimuli. As a general trend, the presence of additional guanosine residues at the terminal positions of sg-HPRT1-G4b and sg-HPRT1-G4c enhanced their sensitivity to chemical stimuli compared with sg-HPRT1-G4a (Figure 4E; Supplementary Figure S12B). Complete inhibition of sg-HPRT1-G4c-supported cleavage of target DNA was achieved by PDP and PDS at 4.0 and 2.0 μM, respectively (Supplementary Figure S12C). Additional studies demonstrated that these criteria are common for different target sequences (Supplementary Figures S13 and S14). Given the large size of G4 ligands, it is likely that proximity and steric effects interfered with the availability of the structural units for sgRNA–dCas9 interactions.

The activities of sequence-modified tracrRNAs were found to be in good agreement with the experimentally obtained sgRNA results (Figure 4F; Supplementary Figures S15–S17). Moreover, the presence of extra guanosine at the 5′ end of the G4-tracrRNAs caused significant enhancement in their sensitivity to chemical stimuli (Figure 4F; Supplementary Figures S16C and S17C). Taken together,

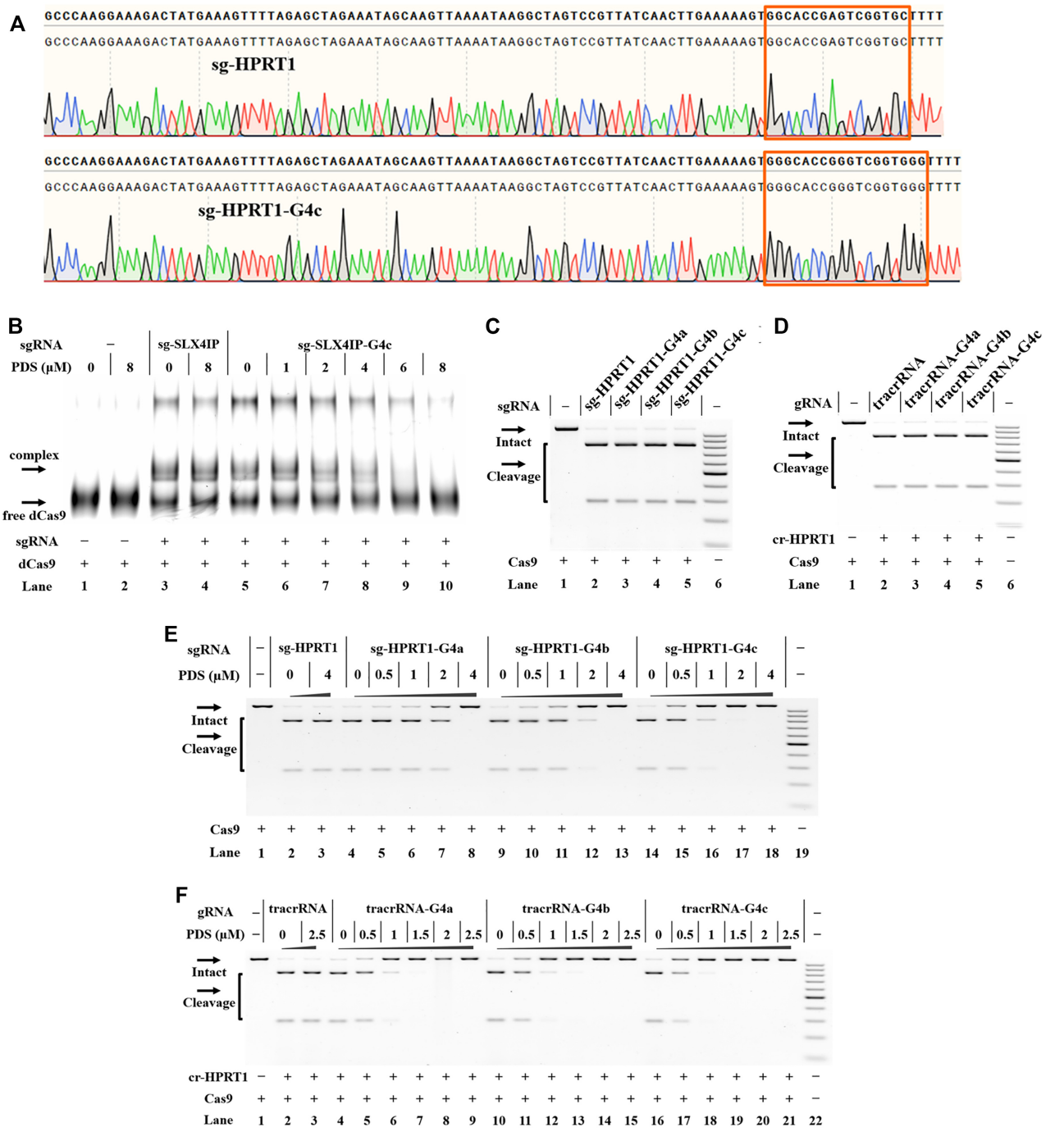

Figure 4. Chemical targeting of G4-gRNAs for modulating CRISPR/Cas9 reactions was performed as described in the Materials and methods. All samples were tested in three biological replicates. An image of representative data is shown here. (**A**) Sanger sequencing of different sgRNAs. The sites of engineering are indicated. In this study, different sgRNA transcripts were reverse transcribed, PCR amplified and then cloned into a T-vector for sequencing analysis. (**B**) EMSA of fluorescently labeled dCas9 with different sgRNAs in the absence or presence of PDS. The band over the complex may indicate the formation of the protein dimer. Lanes 1–2, dCas9-only control; lanes 3–4, dCas9 and original sg-SLX4IP; lanes 5–10, dCas9 and sg-SLX4IP-G4c. (**C**) The tolerance of Cas9 to each G4-sgRNA. Lane 1, Cas9-only control; lane 2, original sg-HPRT1; lanes 3–5, different G4-sgRNAs; lane 6, DNA marker (GeneRuler 100 bp DNA Ladder). (**D**) The tolerance of Cas9 to each G4-tracrRNA. Lane 1, Cas9-only control; lane 2, cr-HPRT1 and original tracrRNA; lanes 3–5, cr-HPRT1 and different G4-tracrRNAs; lane 6, DNA marker. (**E**) Chemical targeting of G4-sgRNAs for modulating CRISPR/Cas9. Lane 1, Cas9-only control; lanes 2–3, original sg-HPRT1; lanes 4–8, sg-HPRT1-G4a; lanes 9–13, sg-HPRT1-G4b; lanes 14–18, sg-HPRT1-G4c; lane 19, DNA marker. (**F**) Chemical targeting of G4-tracrRNAs for modulating CRISPR/Cas9. Lane 1, Cas9-only control; lanes 2–3, cr-HPRT1 and original tracrRNA; lanes 4–9, cr-HPRT1 and tracrRNA-G4a; lanes 10–15, cr-HPRT1 and tracrRNA-G4b; lanes 16–21, cr-HPRT1 and tracrRNA-G4c; lane 22, DNA marker. For (C) to (F), uncleaved *HPRT1* DNA (1083 bp) and cleaved dsDNA products (803 and 280 bp) are indicated by different arrows.

the binding between stem–loop 3 of gRNA variants and G4 ligands provided an interaction handle for controlling CRISPR/Cas9.

Chemical targeting of IVT G4-sgRNAs for controlling gene editing

The above studies encouraged us to evaluate the efficiency of our strategy to control CRISPR/Cas9-mediated gene editing in human cells. For CRISPR/Cas9-based gene editing study, both Cas9 and gRNA can be introduced into cells in various ways (49). To provide flexibility, the gRNA component can be delivered as either plasmid DNA or IVT RNA (31). We therefore performed cellular studies using a PX165 plasmid containing only the Cas9 expression cassette together with IVT sgRNA transcripts (31). In these studies, the sgRNA sequences (sg-SLX4IP and sg-HPRT1) were the same as that tested for the *in vitro* cleavage assay. We first delivered the PX165 plasmid, followed by the delivery of *HPRT1*-targeting sgRNA 4 h later. Successful gene editing within G4-sgRNA-recipient HeLa cells was confirmed by T7E1 assay of target site-derived PCR amplicons. Taking the *HPRT1*-targeting sgRNAs as examples, the overall activities exhibited by each G4-sgRNA with PX165 were not significantly influenced by altered sequences in stem–loop 3 (Supplementary Figure S18).

We next investigated the effect of chemical targeting of IVT G4-sgRNAs on controlling gene editing in cells. We evaluated the cytotoxic effects of G4 ligands to find the suitable concentrations for use of these molecules. The results demonstrate that HeLa cells can tolerate well up to 8.0 μM PDS after 24 h of incubation (Supplementary Figure S19). We next transfected PX165 plasmids and individual sgRNAs into HeLa cells before the treatment with each G4 ligand. We demonstrated that the amount of indels (insertion/deletion substitutions) formed at target sites decreased in a dose-dependent manner as the concentration of each G4 ligand increased (Figure 5A, B). We also demonstrated that PDS appears to be the more potent compound for modulating gene editing. The variations in activities of these G4 ligands in cells are consistent with the *in vitro* Cas9 studies as they displayed different G4-stabilizing activities toward the G4 motif in engineered sgRNAs. We further demonstrated that these criteria are common for different target sequences (Supplementary Figure S20). We further test the reversibility of small-molecule G4 ligands. It is demonstrated that the cells with media swap at an earlier time point (2 h of incubation) showed less inhibition (Supplementary Figure S21). Hence, PDS can be a reversible inhibitor of G4-forming sgRNAs in cells.

We further performed a Cas9 RNP study using Cas9 protein along with different IVT sgRNAs (50). The results also showed a trend to reduction after G4 ligand treatment (Figure 5C, D). We also benchmarked the performance of our strategy against that of Brd0539 to control gene editing in HeLa cells (17). The Cas9 protein and IVT sgRNAs were delivered into cells as above before either PDS or Brd0539 was added. The amount of indel formation was determined 24 h after the compound treatment. We demonstrated that a relatively lower concentration of PDS exhibits better gene editing inhibition effects in HeLa cells compared with Brd0539.

Chemical targeting of plasmid-encoded G4-sgRNAs for controlling gene editing

In the above studies, two sequential nucleic acid transfection rounds were used to perform gene editing in cells. For the sake of practicality and limiting transfection-associated cytotoxic effects, gene editing protocols do not entail such two-step consecutive nucleic acid transfections. It will be more convenient to perform gene editing by using an all-in-one vector for the expression of sgRNA and Cas9, such as PX459 or its derivatives (31,51). For our purpose, overlap extension PCR and the in-fusion cloning method was used to replace the sgRNA-encoding sequence with the G4-forming fragments in PX459 plasmid. The constructed plasmids were confirmed by sequencing and designated as PX459-G4a, PX459-G4b and PX459-G4c, respectively. Each of these constructs has BbsI cloning sites for the gRNA sequence. We selected two endogenous genes (*SLX4IP* and *HPRT1*) to investigate whether these all-in-one constructs could attain efficient gene editing. In our studies, HeLa cells were transfected with each complete all-in-one plasmid. A complete media change was performed at 4 h post-transfection and cells were cultured for an additional 24 h. Following this, the T7E1 assay was performed and the percentage of indels was determined. We demonstrate that all G4-containing constructs could promote high-level editing of target genes in HeLa cells (Figure 6A, B).

We anticipated that the G4 ligand treatment can drive the formation of RNA G4 and subsequently inhibit the function of plasmid-encoded sgRNAs. HeLa cells were transfected with each all-in-one plasmid and were then incubated with different concentrations of each G4 ligand. At 24 h post-treatment, the cells were harvested to analyze the gene editing efficiencies. Strikingly, we found that each G4 ligand greatly decreased the ability of G4-containing plasmids to create genome lesions at target sites in HeLa cells (Figure 6C, D; Supplementary Figure S22). Based on the above data, we conclude that G4-sgRNAs with a more stable G4 core exert a more favorable responsiveness to G4 ligand in cells. We further demonstrated that these criteria are common for all-in-one plasmids with different guide sequences (Supplementary Figures S23 and S24). Hence, the activity of the single plasmid-based approach can be modulated with our strategy of rational gRNA modifications along with the use of G4 ligands.

Chemical targeting of G4-sgRNAs for controlling gene expression in human cells

We proceeded to characterize our strategy for expanded applications to counteract sequence-specific regulation of gene expression in human cells. Transcriptional control is a major mechanism for regulating gene expression. CRISPR activation (CRISPRa), based on the fusion of inactive Cas9 (dCas9) to a synthetic transcriptional activator (VP64), provides a useful tool set for activating gene expression (52). It is important to regulate this multifunctional system so that

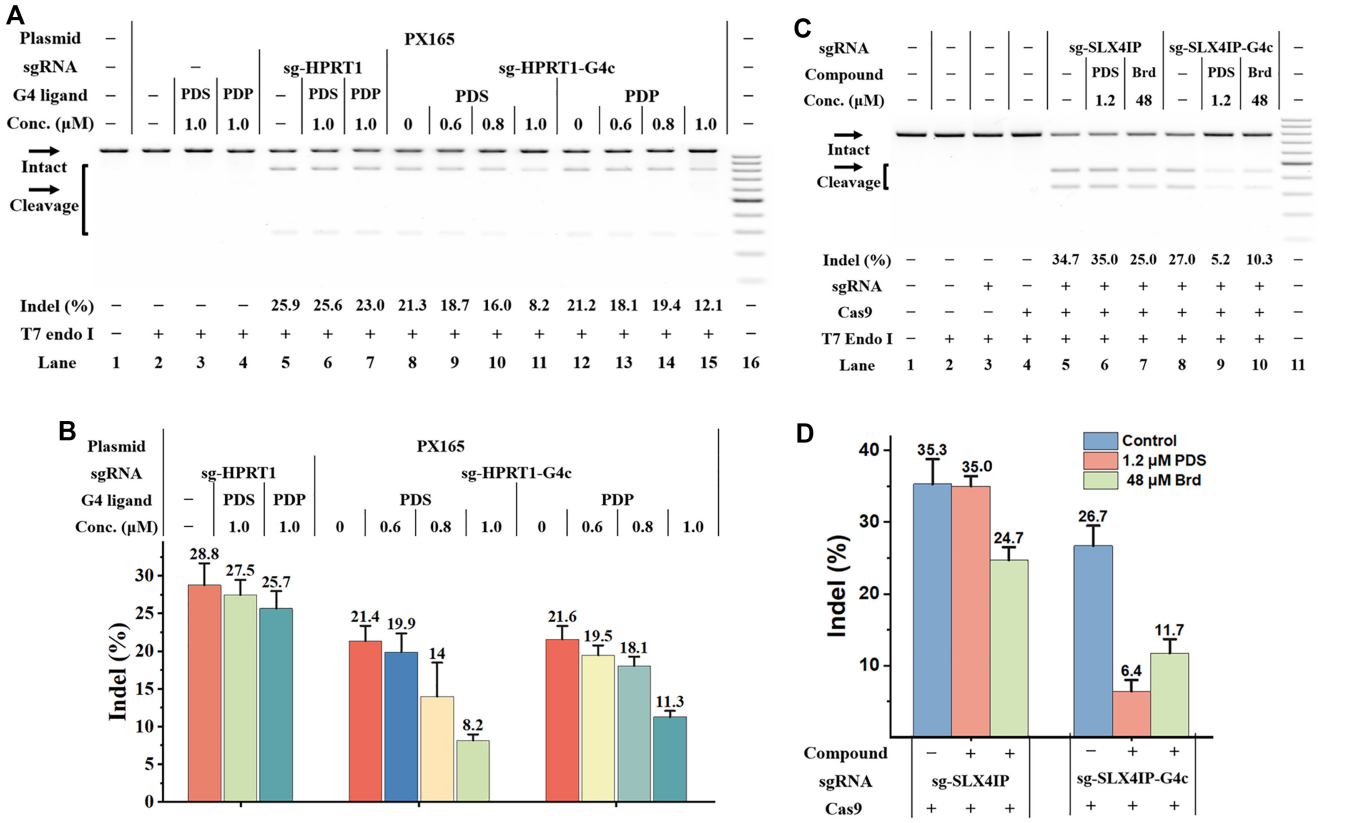

Figure 5. Chemical targeting of IVT G4-sgRNAs for controlling gene editing. Cellular studies were performed as described in the Materials and methods. Amplicon substrates and T7E1 cleavage products are indicated by different arrowheads. All samples were tested in three biological replicates. An image of representative data is shown here. (**A**) Chemical targeting of IVT G4-sgRNAs for modulating gene editing in HeLa cells. The PX165 plasmids and IVT sgRNAs were delivered into HeLa cells before the treatment with each G4 ligand. Uncleaved HPRT1 DNA (1083 bp) cut to shorter cleavage fragments (803 and 280 bp) is demonstrated. Lane 1, target control; lanes 2–4, PX165 control; lanes 5–7, PX165 and original sg-HPRT1; lanes 8–11 and 12–15, PX165 and sg-HPRT1-G4c; lane 16, DNA marker (GeneRuler 100 bp DNA Ladder). (**B**) Statistical treatment of three replicates with indel quantifications. (**C**) Cas9 RNP study of using Cas9 protein along with different IVT sgRNAs. Uncleaved SLX4IP DNA (773 bp) cut to shorter cleavage fragments (441 and 332 bp) is demonstrated. Lane 1, target control; lane 2, T7 endo I control; lane 3, sgRNA-only control; lane 4, Cas9-only control; lanes 5–7, Cas9/sg-SLX4IP; lanes 8–10, Cas9/sg-SLX4IP-G4c; lane 11, DNA marker. (**D**) Statistical treatment of three replicates with indel quantifications. For (B) and (D), data represent the mean of three replicates and are shown as mean ± SEM.

the target genes are only active when they are needed. A peptide-based scaffold recruitment system is chosen to facilitate the analysis (8). The dCas9-SunTag-VP64 expression plasmids were used with either the wild-type sgRNA or G4-sgRNA for achieving transcriptional activation of DNA target sites of interest. We demonstrate that the dCas9-SunTag system utilizing the G4-sgRNAs drives robust and specific activation of the *CXCR4* (C-X-C Chemokine Receptor 4) gene (Figure 7A) (8). We further tested the effects of G4 targeting on this system. The dCas9-SunTag-VP64 expression plasmids and IVT G4-sgRNAs were delivered into cells before treatment with PDS. Consistent with gene editing studies, the presence of extra G sites in G4-sgRNAs caused significant enhancement in their sensitivity to chemical stimuli (sg-CXCR4-G4b, sg-CXCR4-G4c, Figure 7A).

In contrast to CRISPRa, CRISPR deactivation delivers a gene repression mechanism by recruiting a transcription repression module (the Krüppel-associated box domain, KRAB) (53,54). We envisaged that chemical targeting of G4-sgRNAs can be used to control the function of KRAB repressor and the GCN4 SunTag scaffold. We delivered the G4-sgRNAs 4 h after the transfection of dCas9-SunTag-KRAB expression plasmids, and total RNAs were extracted and analyzed 24 h later. We demonstrated that robust transcriptional inhibition can be achieved through targeting of dCas9-SunTag-KRAB with G4-sgRNAs. We further demonstrated that chemical targeting of G4-sgRNAs functions well to reduce the ability of dCas9-SunTag-KRAB to target *CXCR4* transcription (Figure 7B). These results together demonstrated that chemical targeting of G4-sgRNAs could introduce more regulatory scope for conditional control of gene expression at target sites in the genome.

DISCUSSION

The current study presents a novel bioinformatic and experimental approach for interrogating functional tolerance of gRNA scaffolds in a predictive manner. We explore a concept whereby G4 ligands known to bind to and intercalate in G4 nucleic acids, are evaluated for disrupting the Cas9 interaction with G4-gRNA scaffolds. In doing so, specific ligand binding to G4-gRNAs seeks to reduce (ideally block) DNA cleavage activity. The use of G4 ligands for targeting RNA

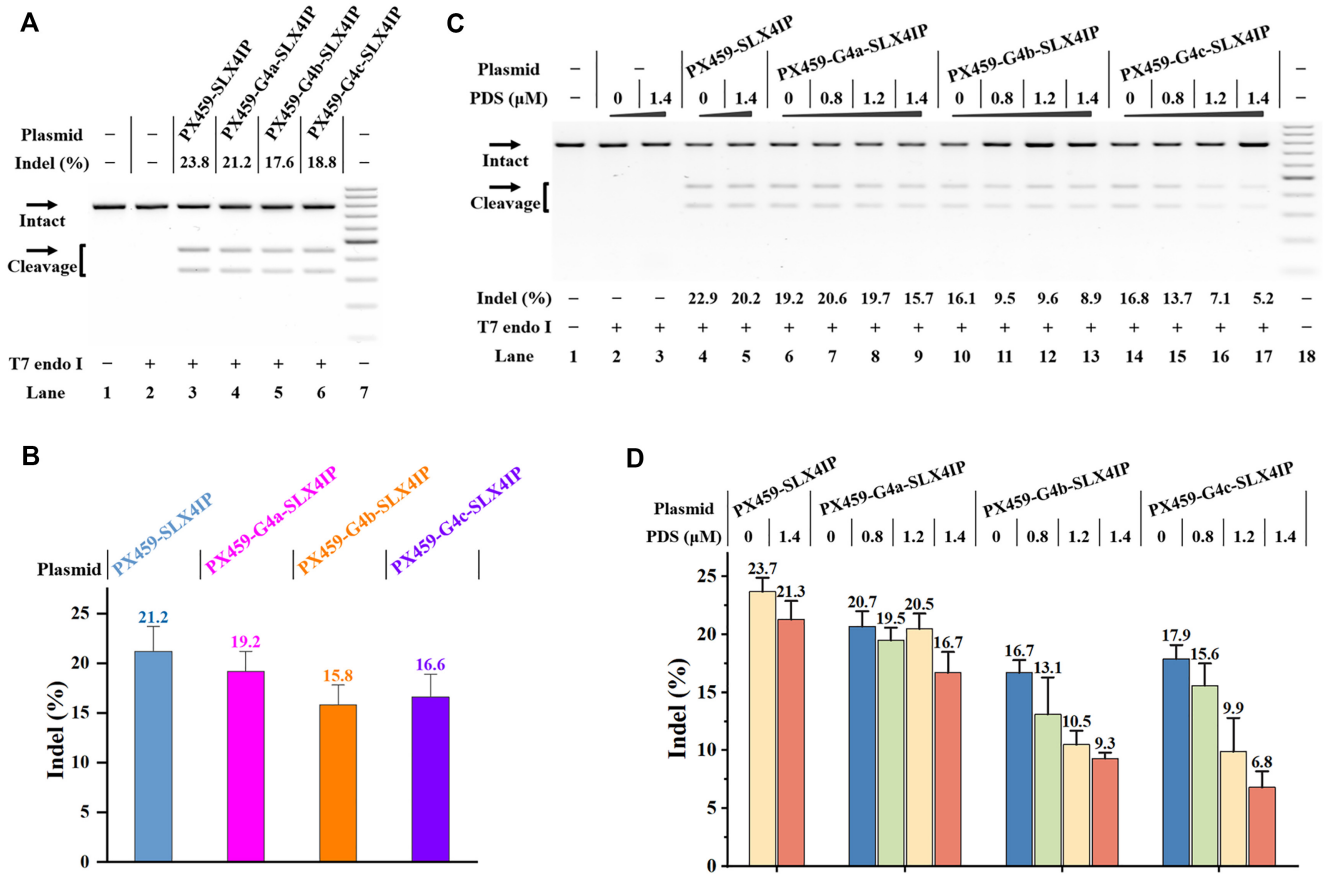

Figure 6. Chemical targeting of plasmid-encoded G4-sgRNAs for controlling gene editing. Cellular studies were performed as described in the Materials and methods. The all-in-one plasmids were delivered into HeLa cells before the treatment with PDS. Amplicon substrates and T7E1 cleavage products are indicated by different arrowheads. All samples were tested in three biological replicates. An image of representative data is shown here. (**A**) Editing of the SLX4IP gene in HeLa cells using the indicated all-in-one plasmids. Lane 1, target control; lane 2, T7 endo I control; lane 3, PX459-SLX4IP; lane 4, PX459-G4a-SLX4IP; lane 5, PX459-G4b-SLX4IP; lane 6, PX459-G4c-SLX4IP; lane 7, DNA marker (GeneRuler 100 bp DNA Ladder). (**B**) Statistical treatment of three replicates with indel quantifications. (**C**) Chemical targeting of all-in-one plasmid-encoded G4-sgRNAs for modulating gene editing in HeLa cells. Lane 1, target control; lanes 2–3, T7 endo I control; lanes 4–5, PX459-SLX4IP; lanes 6–9, PX459-G4a-SLX4IP; lanes 10–13, PX459-G4b-SLX4IP; lanes 14–17, PX459-G4c-SLX4IP; lane 18, DNA marker. (**D**) Statistical treatment of three replicates with indel quantifications. For (A) and (C), uncleaved *SLX4IP* DNA (773 bp) cut to shorter cleavage fragments (441 and 332 bp) is demonstrated. For (B) and (D), the data are presented as the means ± SEM from three independent experiments.

or DNA structures is quite traditional but not reported for CRISPR applications prior to this study (24). This study involves a stepwise progression of stages from *in vitro* designing and testing of different designed gRNAs and several G4 ligands, and subsequent *in cellulo* testing, using transfection of selected IVT gRNA reagents and, at the end, designer RNA-encoding DNA constructs. This study possibly indicates that the identity of some nucleotides in sgRNAs is not strictly conserved. This study lays the foundation for the rapid identification and use of small-molecule inhibitors against CRISPR/Cas9. In general, our strategy has the advantage of being inexpensive and technically easy. A particularly valuable aspect of this approach is its amenability to ligand control over CRISPR/Cas9 activity using genetically encoded G4-gRNAs.

Here, we establish a modular platform for engineering gRNAs and demonstrate the applicability of such constructs for controlling gene editing and expression in cells. Although protein engineering has yielded many useful proteins for biomedical applications (55,56), RNA engineering has received much less attention in the field of chemical biology (57). One of the key restrictions in RNA engineering has been the lack of detailed structural knowledge of an RNA sequence. For controlling CRISPR/Cas9, the engineering of gRNA is more feasible because the molecular basis for Cas9 function is not well understood and cannot be engineered rationally. Functional gRNA contains multiple well-defined structural motifs, which are important for interaction with Cas9 to form functional gRNA–protein complexes. Sequence analysis is performed for decrypting the G4-forming potential of these structural motifs present in gRNAs. Stem–loop 3 with the highest G content in the scaffold sequence is selected for the current engineering study. Part of the reason for this is that a high G content will result in a relatively higher G4-forming propensity, which might make it easy to uniquely engineer such a sequence into a G4-forming unit. The sequence-modified gRNAs can still maintain the overall structural and chemical identity of the

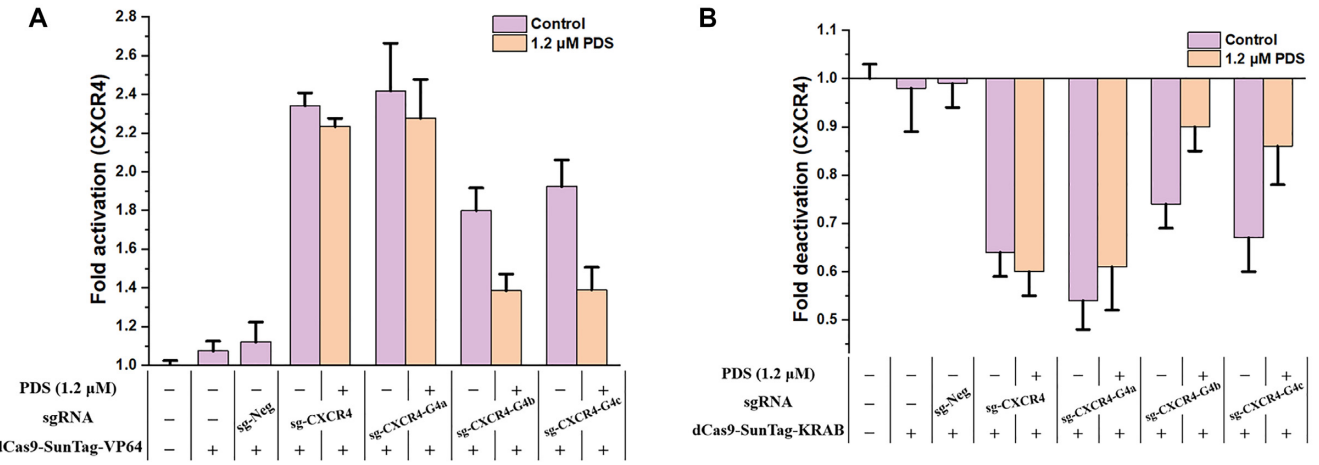

Figure 7. Chemical targeting of G4-sgRNAs for modulating gene expression in human cells. Cellular studies were performed as described in the Materials and methods. The plasmids and sgRNAs were delivered into HeLa cells before the treatment with PDS. All samples were tested in three biological replicates. The data are presented as the means ± SEM from three independent experiments. (**A**) Change in mean expression of *CXCR4* in HeLa cells with dCas9-SunTag-VP64 (+sg-CXCR4) and in the presence and absence of PDS. (**B**) Change in mean expression of *CXCR4* in HeLa cells with dCas9-SunTag-KRAB (+sg-CXCR4) and in the presence and absence of PDS.

original gRNAs. The overall tolerance of the gRNA scaffold to a variety of substitutions in stem–loop 3 is an important attribute for its potential as a molecular scaffold.

Among various non-canonical nucleic acid structures, G4 motifs have attracted great research attention as prospective targets for the chemical intervention in biological functions (36,58,59). The current study included the examination of PDS and its bisquinolinium derivative (PDP) that are closely related to each other. It is demonstrated that PDS is more effective to suppress the function of G4-gRNA function than PDP. However, small differences in their chemical structures account for the fact that there is not a great difference in potency between PDP and PDS. There are two possible mechanisms to explain the interaction between Cas9 and gRNA in the presence of G4 ligands. It is possible that the complex formation of Cas9 and gRNA was inhibited by G4 formation due to ligand binding. The other possible mechanism is that the complex formation and activities of Cas9 were inhibited by G4 liands bound to the G4 structure. Although G4 ligands were shown to have potential pharmacological value, a significant limitation in applying G4 ligands to biological studies is their toxicity to human cells (60,61). One of the possible reasons is that G4 motifs are abundant in specific chromosomal domains (62). At this stage, in contrast to the well-developed anti-CRISPR proteins (16,63), there is still room for further growth and improvement in the generation of G4 ligands that bind selectively to target gRNA motifs. Rational design of G4 ligands will also benefit from the growing availability of G4 structural and biochemical data, molecular modeling and simulation.

CONCLUSIONS

The rich structural diversity of RNAs offers a reservoir of targets for small molecules to bind, thus creating the potential to modulate RNA biology.

DATA AVAILABILITY

The data that support the findings of this study are available in the Supplementary Data of this article. Further information and requests for resources and reagents should be directed to and will be fulfilled by the lead contact, Tian Tian (ttian@whu.edu.cn).

SUPPLEMENTARY DATA

Supplementary Data are available at NAR Online.

ACKNOWLEDGEMENTS

The authors thank Professor Ping Yin (Huazhong Agricultural University) and Professor Shaoru Wang (Wuhan University) for their valuable help.
Author contributions: T.T. conceived the original idea, designed the studies and led the project. X.Y.L., S.Y.C. and Q.Q.Q. performed all biological studies. H.J.L., Y.T.Z., W.S. and F.F. contributed to *in vitro* Cas9 studies. X.Z. provided consistent support during the running of this project. T.T. wrote the manuscript. All the authors provided feedback on the study and on the manuscript.

FUNDING

The National Natural Science Foundation of China [22177089, 91853119, 21721005, 91753201, 21877086 and 22177088]; the Hubei Natural Science Foundation for Distinguished Young Scholars [2019CFA064]; and Fundamental Research Funds for the Central Universities [2042019kf0189]. Funding for open access charge: National Natural Science Foundation of China.
Conflict of interest statement. The authors declare no competing financial interests.

REFERENCES

1. Mojica,F.J., Diez-Villasenor,C., Soria,E. and Juez,G. (2000) Biological significance of a family of regularly spaced repeats in the genomes of archaea, bacteria and mitochondria. *Mol. Microbiol.*, **36**, 244–246.
2. Jinek,M., Chylinski,K., Fonfara,I., Hauer,M., Doudna,J.A. and Charpentier,E. (2012) A programmable dual-RNA-guided DNA endonuclease in adaptive bacterial immunity. *Science*, **337**, 816–821.
3. Cong,L., Ran,F.A., Cox,D., Lin,S., Barretto,R., Habib,N., Hsu,P.D., Wu,X., Jiang,W., Marraffini,L.A. *et al.* (2013) Multiplex genome engineering using CRISPR/Cas systems. *Science*, **339**, 819–823.
4. Mali,P., Yang,L., Esvelt,K.M., Aach,J., Guell,M., DiCarlo,J.E., Norville,J.E. and Church,G.M. (2013) RNA-guided human genome engineering via cas9. *Science*, **339**, 823–826.
5. Doudna,J.A. and Charpentier,E. (2014) Genome editing. The new frontier of genome engineering with CRISPR-Cas9. *Science*, **346**, 1258096.
6. Qi,L.S., Larson,M.H., Gilbert,L.A., Doudna,J.A., Weissman,J.S., Arkin,A.P. and Lim,W.A. (2013) Repurposing CRISPR as an RNA-guided platform for sequence-specific control of gene expression. *Cell*, **152**, 1173–1183.
7. Nunez,J.K., Chen,J., Pommier,G.C., Cogan,J.Z., Replogle,J.M., Adriaens,C., Ramadoss,G.N., Shi,Q., Hung,K.L., Samelson,A.J. *et al.* (2021) Genome-wide programmable transcriptional memory by CRISPR-based epigenome editing. *Cell*, **184**, 2503–2519.
8. Tanenbaum,M.E., Gilbert,L.A., Qi,L.S., Weissman,J.S. and Vale,R.D. (2014) A protein-tagging system for signal amplification in gene expression and fluorescence imaging. *Cell*, **159**, 635–646.
9. Senturk,S., Shirole,N.H., Nowak,D.G., Corbo,V., Pal,D., Vaughan,A., Tuveson,D.A., Trotman,L.C., Kinney,J.B. and Sordella,R. (2017) Rapid and tunable method to temporally control gene editing based on conditional cas9 stabilization. *Nat. Commun.*, **8**, 14370.
10. Luo,J., Liu,Q., Morihiro,K. and Deiters,A. (2016) Small-molecule control of protein function through Staudinger reduction. *Nat. Chem.*, **8**, 1027–1034.
11. Jain,P.K., Ramanan,V., Schepers,A.G., Dalvie,N.S., Panda,A., Fleming,H.E. and Bhatia,S.N. (2016) Development of light-activated CRISPR using guide RNAs with photocleavable protectors. *Angew. Chem. Int. Ed. Engl.*, **55**, 12440–12444.
12. Hemphill,J., Borchardt,E.K., Brown,K., Asokan,A. and Deiters,A. (2015) Optical control of CRISPR/Cas9 gene editing. *J. Am. Chem. Soc.*, **137**, 5642–5645.
13. Moroz-Omori,E.V., Satyapertiwi,D., Ramel,M.C., Hogset,H., Sunyovszki,I.K., Liu,Z., Wojciechowski,J.P., Zhang,Y., Grigsby,C.L., Brito,L. *et al.* (2020) Photoswitchable gRNAs for spatiotemporally controlled CRISPR-Cas-based genomic regulation. *ACS Cent. Sci.*, **6**, 695–703.
14. Clarke,R., Terry,A.R., Pennington,H., Hasty,C., MacDougall,M.S., Regan,M. and Merrill,B.J. (2021) Sequential activation of guide RNAs to enable successive CRISPR-Cas9 activities. *Mol. Cell*, **81**, 226–238.
15. Kundert,K., Lucas,J.E., Watters,K.E., Fellmann,C., Ng,A.H., Heineike,B.M., Fitzsimmons,C.M., Oakes,B.L., Qu,J., Prasad,N. *et al.* (2019) Controlling CRISPR-Cas9 with ligand-activated and ligand-deactivated sgRNAs. *Nat. Commun.*, **10**, 2127.
16. Pawluk,A., Amrani,N., Zhang,Y., Garcia,B., Hidalgo-Reyes,Y., Lee,J., Edraki,A., Shah,M., Sontheimer,E.J., Maxwell,K.L. *et al.* (2016) Naturally occurring off-switches for CRISPR-Cas9. *Cell*, **167**, 1829–1838.
17. Maji,B., Gangopadhyay,S.A., Lee,M., Shi,M., Wu,P., Heler,R., Mok,B., Lim,D., Siriwardena,S.U., Paul,B. *et al.* (2019) A high-throughput platform to identify small-molecule inhibitors of CRISPR-Cas9. *Cell*, **177**, 1067–1079.
18. Zou,R.S., Liu,Y., Wu,B. and Ha,T. (2021) Cas9 deactivation with photocleavable guide RNAs. *Mol. Cell*, **81**, 1553–1565.
19. Nishimasu,H., Ran,F.A., Hsu,P.D., Konermann,S., Shehata,S.I., Dohmae,N., Ishitani,R., Zhang,F. and Nureki,O. (2014) Crystal structure of cas9 in complex with guide RNA and target DNA. *Cell*, **156**, 935–949.
20. Yamada,M., Watanabe,Y., Gootenberg,J.S., Hirano,H., Ran,F.A., Nakane,T., Ishitani,R., Zhang,F., Nishimasu,H. and Nureki,O. (2017) Crystal structure of the minimal cas9 from *Campylobacter jejuni* reveals the molecular diversity in the CRISPR-Cas9 systems. *Mol. Cell*, **65**, 1109–1121.
21. Costales,M.G., Childs-Disney,J.L., Haniff,H.S. and Disney,M.D. (2020) How we think about targeting RNA with small molecules. *J. Med. Chem.*, **63**, 8880–8900.
22. Bugaut,A., Murat,P. and Balasubramanian,S. (2012) An RNA hairpin to G-quadruplex conformational transition. *J. Am. Chem. Soc.*, **134**, 19953–19956.
23. Kuo,M.H., Wang,Z.F., Tseng,T.Y., Li,M.H., Hsu,S.T., Lin,J.J. and Chang,T.C. (2015) Conformational transition of a hairpin structure to G-quadruplex within the WNT1 gene promoter. *J. Am. Chem. Soc.*, **137**, 210–218.
24. Varshney,D., Spiegel,J., Zyner,K., Tannahill,D. and Balasubramanian,S. (2020) The regulation and functions of DNA and RNA G-quadruplexes. *Nat. Rev. Mol. Cell Biol.*, **21**, 459–474.
25. Herdy,B., Mayer,C., Varshney,D., Marsico,G., Murat,P., Taylor,C., D'Santos,C., Tannahill,D. and Balasubramanian,S. (2018) Analysis of NRAS RNA G-quadruplex binding proteins reveals DDX3X as a novel interactor of cellular G-quadruplex containing transcripts. *Nucleic Acids Res.*, **46**, 11592–11604.
26. Lyu,K., Chow,E.Y., Mou,X., Chan,T.F. and Kwok,C.K. (2021) RNA G-quadruplexes (rG4s): genomics and biological functions. *Nucleic Acids Res.*, **49**, 5426–5450.
27. Grand,C.L., Han,H., Munoz,R.M., Weitman,S., Von Hoff,D.D., Hurley,L.H. and Bearss,D.J. (2002) The cationic porphyrin TMPyP4 down-regulates c-MYC and human telomerase reverse transcriptase expression and inhibits tumor growth in vivo. *Mol. Cancer Ther.*, **1**, 565–573.
28. Muller,S., Kumari,S., Rodriguez,R. and Balasubramanian,S. (2010) Small-molecule-mediated G-quadruplex isolation from human cells. *Nat. Chem.*, **2**, 1095–1098.
29. Kumari,S., Bugaut,A., Huppert,J.L. and Balasubramanian,S. (2007) An RNA G-quadruplex in the 5′ UTR of the NRAS proto-oncogene modulates translation. *Nat. Chem. Biol.*, **3**, 218–221.
30. Muller,S., Sanders,D.A., Di Antonio,M., Matsis,S., Riou,J.F., Rodriguez,R. and Balasubramanian,S. (2012) Pyridostatin analogues promote telomere dysfunction and long-term growth inhibition in human cancer cells. *Org. Biomol. Chem.*, **10**, 6537–6546.
31. Ran,F.A., Hsu,P.D., Wright,J., Agarwala,V., Scott,D.A. and Zhang,F. (2013) Genome engineering using the CRISPR-Cas9 system. *Nat. Protoc.*, **8**, 2281–2308.
32. Zhou,Y., Zhu,S., Cai,C., Yuan,P., Li,C., Huang,Y. and Wei,W. (2014) High-throughput screening of a CRISPR/Cas9 library for functional genomics in human cells. *Nature*, **509**, 487–491.
33. Dykstra,P.B., Kaplan,M. and Smolke,C.D. (2022) Engineering synthetic RNA devices for cell control. *Nat. Rev. Genet.*, **23**, 215–228.
34. Fay,M.M., Lyons,S.M. and Ivanov,P. (2017) RNA G-quadruplexes in biology: principles and molecular mechanisms. *J. Mol. Biol.*, **429**, 2127–2147.
35. Del Villar-Guerra,R., Trent,J.O. and Chaires,J.B. (2018) G-Quadruplex secondary structure obtained from circular dichroism spectroscopy. *Angew. Chem. Int. Ed. Engl.*, **57**, 7171–7175.
36. Zhang,Y., Yang,M., Duncan,S., Yang,X., Abdelhamid,M.A.S., Huang,L., Zhang,H., Benfey,P.N., Waller,Z.A.E. and Ding,Y. (2019) G-quadruplex structures trigger RNA phase separation. *Nucleic Acids Res.*, **47**, 11746–11754.
37. Balagurumoorthy,P., Brahmachari,S.K., Mohanty,D., Bansal,M. and Sasisekharan,V. (1992) Hairpin and parallel quartet structures for telomeric sequences. *Nucleic Acids Res.*, **20**, 4061–4067.
38. Woodson,S.A. and Koculi,E. (2009) Analysis of RNA folding by native polyacrylamide gel electrophoresis. *Methods Enzymol.*, **469**, 189–208.
39. Edwards,D.N., Machwe,A., Wang,Z. and Orren,D.K. (2014) Intramolecular telomeric G-quadruplexes dramatically inhibit DNA synthesis by replicative and translesion polymerases, revealing their potential to lead to genetic change. *PloS One*, **9**, e80664.
40. Martadinata,H. and Phan,A.T. (2009) Structure of propeller-type parallel-stranded RNA G-quadruplexes, formed by human telomeric RNA sequences in K+ solution. *J. Am. Chem. Soc.*, **131**, 2570–2578.
41. Mathad,R.I., Hatzakis,E., Dai,J. and Yang,D. (2011) c-MYC promoter G-quadruplex formed at the 5′-end of NHE III1 element: insights into biological relevance and parallel-stranded G-quadruplex stability. *Nucleic Acids Res.*, **39**, 9023–9033.

42. Amrane,S., Kerkour,A., Bedrat,A., Vialet,B., Andreola,M.L. and Mergny,J.L. (2014) Topology of a DNA G-quadruplex structure formed in the HIV-1 promoter: a potential target for anti-HIV drug development. *J. Am. Chem. Soc.*, **136**, 5249–5252.
43. Gasperini,M., Findlay,G.M., McKenna,A., Milbank,J.H., Lee,C., Zhang,M.D., Cusanovich,D.A. and Shendure,J. (2017) CRISPR/Cas9-mediated scanning for regulatory elements required for HPRT1 expression via thousands of large, programmed genomic deletions. *Am. J. Hum. Genet.*, **101**, 192–205.
44. Panier,S., Maric,M., Hewitt,G., Mason-Osann,E., Gali,H., Dai,A., Labadorf,A., Guervilly,J.H., Ruis,P., Segura-Bayona,S. *et al.* (2019) SLX4IP antagonizes promiscuous BLM activity during ALT maintenance. *Mol. Cell*, **76**, 27–43.
45. Liu,L., Li,X., Ma,J., Li,Z., You,L., Wang,J., Wang,M., Zhang,X. and Wang,Y. (2017) The molecular architecture for RNA-guided RNA cleavage by cas13a. *Cell*, **170**, 714–726.
46. Mekler,V., Minakhin,L. and Severinov,K. (2017) Mechanism of duplex DNA destabilization by RNA-guided cas9 nuclease during target interrogation. *Proc. Natl Acad. Sci. USA*, **114**, 5443–5448.
47. Deng,W., Shi,X., Tjian,R., Lionnet,T. and Singer,R.H. (2015) CASFISH: CRISPR/Cas9-mediated in situ labeling of genomic loci in fixed cells. *Proc. Natl Acad. Sci. USA*, **112**, 11870–11875.
48. Heler,R., Samai,P., Modell,J.W., Weiner,C., Goldberg,G.W., Bikard,D. and Marraffini,L.A. (2015) Cas9 specifies functional viral targets during CRISPR-Cas adaptation. *Nature*, **519**, 199–202.
49. Qiu,M., Glass,Z., Chen,J., Haas,M., Jin,X., Zhao,X., Rui,X., Ye,Z., Li,Y., Zhang,F. *et al.* (2021) Lipid nanoparticle-mediated codelivery of cas9 mRNA and single-guide RNA achieves liver-specific in vivo genome editing of *Angptl3*. *Proc. Natl Acad Sci. USA*, **118**, e2020401118.
50. Zhang,S., Shen,J., Li,D. and Cheng,Y. (2021) Strategies in the delivery of cas9 ribonucleoprotein for CRISPR/Cas9 genome editing. *Theranostics*, **11**, 614–648.
51. Liu,C., Zhang,L., Liu,H. and Cheng,K. (2017) Delivery strategies of the CRISPR-Cas9 gene-editing system for therapeutic applications. *J. Control. Release*, **266**, 17–26.
52. Perez-Pinera,P., Kocak,D.D., Vockley,C.M., Adler,A.F., Kabadi,A.M., Polstein,L.R., Thakore,P.I., Glass,K.A., Ousterout,D.G., Leong,K.W. *et al.* (2013) RNA-guided gene activation by CRISPR-Cas9-based transcription factors. *Nat. Methods*, **10**, 973–976.
53. Yeo,N.C., Chavez,A., Lance-Byrne,A., Chan,Y., Menn,D., Milanova,D., Kuo,C.C., Guo,X., Sharma,S., Tung,A. *et al.* (2018) An enhanced CRISPR repressor for targeted mammalian gene regulation. *Nat. Methods*, **15**, 611–616.
54. Nakamura,M., Srinivasan,P., Chavez,M., Carter,M.A., Dominguez,A.A., La Russa,M., Lau,M.B., Abbott,T.R., Xu,X., Zhao,D. *et al.* (2019) Anti-CRISPR-mediated control of gene editing and synthetic circuits in eukaryotic cells. *Nat. Commun.*, **10**, 194.
55. Rees,H.A., Komor,A.C., Yeh,W.H., Caetano-Lopes,J., Warman,M., Edge,A.S.B. and Liu,D.R. (2017) Improving the DNA specificity and applicability of base editing through protein engineering and protein delivery. *Nat. Commun.*, **8**, 15790.
56. Davis,K.M., Pattanayak,V., Thompson,D.B., Zuris,J.A. and Liu,D.R. (2015) Small molecule-triggered cas9 protein with improved genome-editing specificity. *Nat. Chem. Biol.*, **11**, 316–318.
57. Liang,J.C., Bloom,R.J. and Smolke,C.D. (2011) Engineering biological systems with synthetic RNA molecules. *Mol. Cell*, **43**, 915–926.
58. Kharel,P., Becker,G., Tsvetkov,V. and Ivanov,P. (2020) Properties and biological impact of RNA G-quadruplexes: from order to turmoil and back. *Nucleic Acids Res.*, **48**, 12534–12555.
59. Bugaut,A. and Balasubramanian,S. (2012) 5′-UTR RNA G-quadruplexes: translation regulation and targeting. *Nucleic Acids Res.*, **40**, 4727–4741.
60. De Magis,A., Manzo,S.G., Russo,M., Marinello,J., Morigi,R., Sordet,O. and Capranico,G. (2019) DNA damage and genome instability by G-quadruplex ligands are mediated by r loops in human cancer cells. *Proc. Natl Acad. Sci. USA*, **116**, 816–825.
61. Ruggiero,E. and Richter,S.N. (2018) G-quadruplexes and G-quadruplex ligands: targets and tools in antiviral therapy. *Nucleic Acids Res.*, **46**, 3270–3283.
62. Zyner,K.G., Mulhearn,D.S., Adhikari,S., Martinez Cuesta,S., Di Antonio,M., Erard,N., Hannon,G.J., Tannahill,D. and Balasubramanian,S. (2019) Genetic interactions of G-quadruplexes in humans. *Elife*, **8**, 4693.
63. Pawluk,A., Davidson,A.R. and Maxwell,K.L. (2018) Anti-CRISPR: discovery, mechanism and function. *Nat. Rev. Microbiol.*, **16**, 12–17.